92 *Chem. Mater.* **2010,** *22,* 92–100
DOI:10.1021/cm902454w

CHEMISTRY OF MATERIALS
Article

Nickel and Nickel-Based Nanoalloy Thin Films from Alcohol-Assisted Chemical Vapor Deposition

Naoufal Bahlawane,*[,†] Peter Antony Premkumar,[†,§] Zhenyu Tian,[⊥,‡] Xin Hong,[‡] Fei Qi,[‡] and Katharina Kohse-Höinghaus[†]

[†]*Department of Chemistry, Bielefeld University, Universitätsstr. 25, D-33615 Bielefeld, Germany and* [‡]*National Synchrotron Radiation Laboratory, University of Science and Technology of China, Hefei, Anhui 230029, People's Republic of China.* [§] *Current address: Plasma and Materials Processing Group, Department of Applied Physics, Eindhoven University of Technology, P.O. Box 513, N-laag c 1.03,. 5600 MB Eindhoven, The Netherlands.* [⊥] *Current address: Département de Chimie Physique des Réactions, UMR 7630 CNRS, INPL-ENSIC 1, rue Grandville, BP 451,54001 Nancy Cedex, France*

Received August 10, 2009. Revised Manuscript Received November 10, 2009

The growth of nickel and nickel-based alloys was investigated using the pulsed-spray evaporation (PSE) CVD process in hydrogen-free atmosphere. This process relies on the reactivity of ethanol, which was investigated using mass spectrometry. In fact, the dehydrogenation of ethanol to form acetaldehyde is identified as the reaction pathway that provides hydrogen atoms necessary to desorb acetylacetonate ligand of the precursor. This global reaction leads to the formation of metallic nickel film either in the hexagonal (hcp) lattice at low temperature or in the cubic (fcc) one at temperatures higher than 240 °C. In conditions where the fcc−Ni phase is deposited, the PSE−CVD process enables the deposition of Ni−Cu alloy thin films with fully controlled composition, whereas Ni−Ag forms polycrystalline silver, in addition to an amorphous phase containing silver and nickel. The synthesis of Ni−Co alloy thin films was performed under conditions where the hcp−Ni phase was obtained, providing for the first time a route toward deposition of nickel-rich hcp−Ni−Co.

Introduction

Nanoalloys, and in particular nickel-based alloys, have attracted a great deal of interest because of their technologically important catalytic, optical, and magnetic properties.[1−3] Forming bimetallic solids is a way to tune the material's properties and to offer prospects for the design of new functionalities. Among the technologically relevant nickel-based alloys, nickel−copper (Ni−Cu), nickel−cobalt (Ni−Co), and nickel−silver (Ni−Ag) find a wide range of applications.

Ni−Cu alloys are efficient catalysts and electrocatalysts for a number of reactions including methane decomposition, methanol oxidation, and $NaBH_4$ hydrolysis to generate hydrogen; in these cases, Cu and Ni exhibit a catalytic synergistic effect.[3,4] The face-centered cubic (fcc) structures of Ni and Cu exhibit a reasonable lattice match to form solid solutions of Ni−Cu in the entire composition range. Van Ingen et al.[5] have demonstrated the synthesis of polycrystalline single phase Cu_xNi_{1-x}, (x = 0−1) thin films using laser ablation deposition, while Zhang et al.[3] have used the thermolysis of the acetylacetonate precursors in oleylamine/1-octadecene to synthesize Cu_xNi_{1-x}, (x = 0−1) nanocrystals. Other wet-chemical processes like electrodeposition[6,7] and the microemulsion route[8] were also used to synthesize nanoalloy thin films and particles.

Ni−Co alloys were theoretically predicted to exhibit superior efficiency as catalysts for the growth of single-walled carbon nanotubes.[9] Other promising applications of Ni−Co alloy thin films include the preparation of micro-levitating magnets.[10] In contrast to Ni−Cu alloys, Ni−Co tends to transit from the fcc phase in nickel-rich solid solutions to the hexagonal close-packed (hcp) structure for cobalt-rich alloys.[11,12] These Ni−Co alloys were synthesized as thin films using electrochemical deposition[10−12]

*Corresponding author. Phone: +49-521 106 2199. Fax: +49-521 106 6027. E-mail: naoufal@pc1.uni-bielefeld.de.

(1) Zhang, Z. Y.; Nenoff, T. M.; Huang, J. Y.; Berry, D. T.; Provencio, P. P. *J. Phys. Chem. C* **2009**, *113*, 1155–1159.
(2) Ferrando, R.; Jellinek, J.; Johnston, R. L. *Chem. Rev.* **2008**, *108*, 845–910.
(3) Zhang, Y. W.; Huang, W. Y.; Habas, S. E.; Kuhn, J. N.; Grass, M. E.; Yamada, Y.; Yang, P.; Somorjai, G. A. *J. Phys. Chem. C* **2008**, *112*, 12092–12095.
(4) Cunha, A. F.; Órfão, J. J. M.; Figueiredo, J. L. *Int. J. Hydrogen Energy* **2009**, *34*, 4763–4772.
(5) Van Ingen, R. P.; Fastenau, R. H. J.; Mittemeijer, E. J. *J. Appl. Phys.* **1994**, *76*, 1871–1883.
(6) Alper, M.; Kockar, H.; Safak, M.; Baykul, M. C. *J. Alloys Compd.* **2008**, *453*, 15–19.
(7) Baskaran, I.; Sankara Narayanan, T. S. N.; Stephen, A. *Mater. Lett.* **2006**, *60*, 1990–1995.
(8) Ahmed, J.; Ramanujachary, K. V.; Lofland, S. E.; Furiato, A.; Gupta, G.; Shivaprasad, S. M.; Ganguli, A. K. *Colloids Surf., A* **2008**, *331*, 206–212.
(9) Deng, W. Q.; Xu, X.; Goddard, W. A. *Nano Lett.* **2004**, *4*, 2331–2335.
(10) Elbuken, C.; Yavuz, M.; Khamesee, M. B. *J. Appl. Phys.* **2008**, *104*, 044905.
(11) Wang, L.; Gao, Y.; Xue, Q.; Liu, H.; Xu, T. *Appl. Surf. Sci.* **2005**, *242*, 326–332.
(12) Qiao, G.; Jing, T.; Wang, N.; Gao, Y.; Zhao, X.; Zhou, J.; Wang, W. *Electrochim. Acta* **2005**, *51*, 85–92.

 Published on Web 12/02/2009

and sputtering[13] or as particles using microemulsion[14] and polyol processes.[15] Nickel-rich Ni−Co alloys exhibit superior efficiency and stability as oxygen-evolution reaction catalyst,[16] whereas cobalt-rich alloys show a markedly high wear resistance and low friction coefficient due to the hcp structure.[11]

Ni and Ag are known to be immiscible for all compositions.[2] Indeed, Zolla and Spaepen[17] have measured a positive heat of mixing of 3.6 kJ/mol for the average alloy composition of 6.89 at.% Ni. However, nonequilibrium Ni−Ag alloys can be synthesized when mild processes are used. Proux et al.[18,19] have investigated Ni−Ag heterogeneous alloys with nickel contents of 10, 15, and 35%, which have been grown at liquid nitrogen temperature using a sputtering technique. These films were composed of pure nickel aggregates statistically distributed in the Ag-rich matrix, a structure that exhibits a marked magnetoresistance even after annealing at 250 °C. Using this deposition process, the authors estimated the maximal solubility of nickel in a silver matrix at 47 at.%.[18,19] In earlier work, Van Ingen et al.,[5,20] have grown Ag−Ni films using laser ablation at room temperature. The authors have shown that obtained films contain, in addition to pure nickel and silver phases, a nonequilibrium Ag_xNi_{1-x} solid solution in which the degree of supersaturation attains 44 at.% of Ag. Kumar et al.[21] have succeeded in reacting silver and nickel nanoparticles at 100 °C to form the alloy phase using the impregnation method.

The previously mentioned processes, however, show limited performance if coating has to be applied to nanostructured three-dimensional surfaces, which are the typical surfaces in high-performance electronic and magnetic applications. This limitation can be overcome with the chemical vapor deposition process (CVD) which is a single-step and high-throughput process. This process is curiously overlooked for the above-mentioned alloys, a fact that is presumably related to the difficulty in handling a dual-source delivery process to adjust the composition, or to the high thermal activation that leads to dealloying. Single-source precursors are easier to handle, but their use limits the flexibility in terms of tuning the film composition. In earlier reports we have demonstrated that pulsed-spray evaporation (PSE) CVD in combination with the alcohol reactivity is an efficient way to grow high quality transition-metal thin films without using hydrogen reduction.[22,23] This development enables the growth of various metals at moderately low temperatures which facilitates the growth of metastable alloys that promise, in general, superior properties. In this study, we present for the first time a systematic study showing the straightforward application of PSE−CVD as a single-pot processing technique to growth technologically relevant nickel-based alloy thin films.

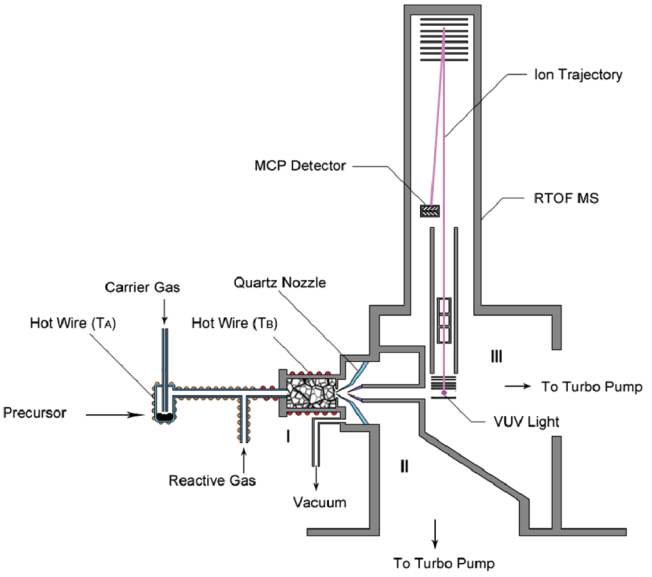

Figure 1. A schematic diagram of the CVD reactor with in situ molecular-beam mass spectrometry. Parts **I**, **II**, and **III** are the CVD reactor, the differential pumped chamber and the photoionization chamber, respectively. The synchrotron VUV light crosses vertically with the molecular beam. The part I was modified to accommodate a pulsed-spray evaporation unit.

Experimental Methods

The deposition of transition metal alloys has been performed on glass substrates using a cold-wall CVD reactor at 50 mbar. During deposition of Ni and Ni-based alloys, a continuous flow of 1 slm of nitrogen was used as carrier gas, whereas the precursor and the ethanol reducing agent were admitted, as a single liquid feedstock, in a pulsed way. The CVD reactor is equipped with a pulsed spray unit, which was used with the frequency of 1 Hz and an opening time of 25 ms resulting in a feeding rate of 2.3 mL/min. The precursor liquid feedstock was prepared by dissolving the metal acetylacetonates ($Cu(acac)_2$, $Co(acac)_2$, or $Ni(acac)_2$) or metal nitrate ($AgNO_3$), with the desired ratios, in ethanol to a total metal concentration of 5×10^{-3} mol/L. The fcc crystal structure was grown in this study at 350 °C whereas a deposition temperature of 190 °C was used to grow the hcp structure of nickel-based alloys. Detailed description of the deposition setup can be found elsewhere.[23]

The morphology and the composition of the deposited films were assessed using scanning electron microscopy (SEM) and energy-dispersive X-ray analysis (EDX), whereas the crystalline phases were identified by X-ray diffraction (XRD). The optical

(13) Tomita, S.; Adachi, H.; Fujii, M.; Hayashi, S. *J. Appl. Phys., Part 1* **2001**, *40*, 6370–6374.
(14) Ahmed, J.; Sharma, S.; Ramanujachary, K. V.; Lofland, S. E.; Ganguli, A. K. *J. Colloid Interface Sci.* **2009**, *336*, 814–819.
(15) Toneguzzo, P.; Viau, G.; Acher, O.; Guillet, F.; Bruneton, E.; Fievet-Vincent, F.; Fievet, F. *J. Mater. Sci.* **2000**, *35*, 3767–3784.
(16) Lian, K.; Thorpe, S. J.; Kirk, D. W. *Electrochim. Acta* **1992**, *37*, 169–175.
(17) Zolla, H. G.; Spaepen, F. *Acta Mater.* **1999**, *47*, 2391–2400.
(18) Proux, O.; Mimault, J.; Revenant-Brizard, C.; Regnard, J. R.; Mevel, B. *J. Phys.: Condens. Matter* **1999**, *11*, 147–162.
(19) Proux, O.; Mimault, J.; Regnard, J. R.; Revenant-Brizard, C.; Mevel, B.; Dieny, B. *J. Phys.: Condens. Matter* **2000**, *12*, 3939–3953.
(20) Van Ingen, R. P.; Fastenau, R. H. J.; Mittemeijer, E. J. *Phys. Rev. Lett.* **1994**, *72*, 3116–3119.
(21) Kumar, A.; Damle, C.; Sastry, M. *Appl. Phys. Lett.* **2001**, *79*, 3314–3316.
(22) Bahlawane, N.; Premkumar, P. A.; Onwuka, K.; Reiss, G.; Kohse-Hoinghaus, K. *Microelectron. Eng.* **2007**, *84*, 2481–2485.
(23) Bahlawane, N.; Premkumar, P. A.; Onwuka, K.; Rott, K.; Reiss, G.; Kohse-Hoinghaus, K. *Surf. Coat. Technol.* **2007**, *201*, 8914–8918.

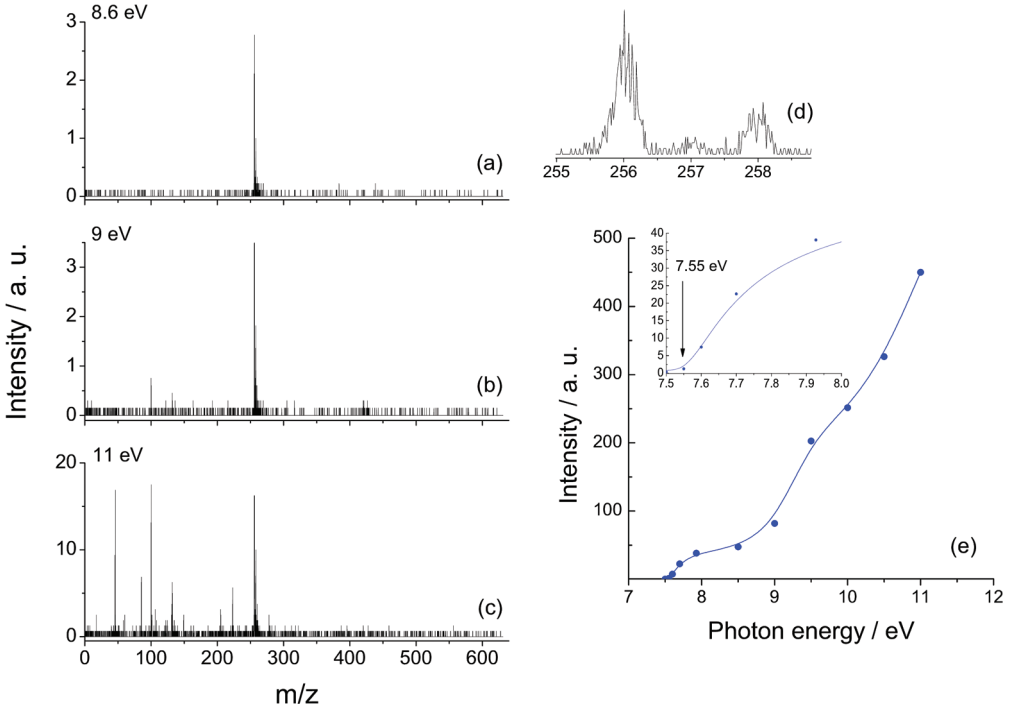

Figure 2. Selected mass spectra (a, b, and c) of nickel acetylacetonate collected using various ionization energies to elucidate the benefit of the tunable ionization energy. The spectrum (d) presents the isotopic distribution of the molecular peak as detected with the ionization energy of 8.6 eV. The plot (e) shows evolution of the intensity of the molecular peak (m/z = 256) as a function of the ionization energy.

reflection was measured using a specular IR reflection cell to monitor the oxidation of metallic deposits and their back-reduction.

In-situ monitoring of the occurring reactions under near-CVD conditions was performed using vacuum ultraviolet (VUV) photoionization mass spectrometry at the National Synchrotron Radiation Laboratory, Hefei, China. As shown in Figure 1, the instrumentation consists of a reactor (**I**), a differentially pumped chamber (**II**) with a molecular-beam sampling system, and a photoionization chamber (**III**) with a reflectron time-of-flight mass spectrometer (RTOF-MS). A newly constructed beamline, using undulator radiation from an 800 MeV electron storage ring, was used for this study. Synchrotron radiation is dispersed by a 1 m Seya-Namioka monochromator equipped with a 1500 grooves/mm grating covering the photon energies from 7.8 to 24 eV. Argon or neon gas filter was used to eliminate the higher-order harmonic radiations. The energy resolving power ($E/\Delta E$) is around 1000 and the average photon flux can reach 10^{13} photons/sec. To cover photon energies below 7.8 eV, a beamline described in ref [24] was used.

A quartz cone-shaped nozzle with a 40° included angle and a ~500 μm orifice at the tip was used to sample reaction species. The nozzle was inserted inside the CVD reactor. The sampled species form a molecular beam in the differentially pumped chamber and pass through a nickel skimmer into the photoionization chamber, where the molecular beam is crossed and ionized by the tunable synchrotron VUV light in the ionization region. Photoions are propelled into the flight tube by a pulse extraction field triggered with a DG 535 pulse generator (Stanford Research Systems, Inc. Sunnyvale, CA) and reflected to a microchannel plate (MCP) detector. After amplification by a VT120C preamplifier (EG&G, ORTEC, Oak Ridge, TN), the ion signal is recorded by a P7888 multiscaler (FAST Comtec, Oberhaching, Germany). A silicon photodiode SXUV-100 (International Radiation Detectors Inc., U.S.) was used to monitor the photon flux for normalizing the ion signals. The pressure in the reactor was set at 16 mbar.

In the present conditions the energy of the incident photons can be tuned to avoid the fragmentation of the precursor, $Ni(acac)_2$, as shown in Figure 2a−e. As illustrated by these spectra, limited fragmentation enables a clear identification of the precursor, and enables for instance to show that the precursor evaporates in the monomer form. These measurements have also shown that no reaction took place between ethanol and the precursor. A slight increase of the photon energy above 9 eV induces a substantial fragmentation so that the investigation of the thermally induced process became challenging.

The result of the ionization energy screening between 7.5 and 12 eV is depicted in Figure 2e. The photoionization threshold of nickel acetylacetonate was measured to be 7.55 eV, which is within the range of the ionization energy measured by photoelectron spectroscopy 7.35−7.62 eV (NIST database) and visibly below the value measured by electron impact techniques (8.23 eV). It is worth mentioning that no data are available for the PI (photoionization mass spectrometry) in the database. The detection of the reaction products was performed by extending the ionization energy up to 16.53 eV.

Results

The growth of metallic thin films from ethanol solution of the corresponding metal acetylacetonate complexes was demonstrated with PSE−CVD in our previous studies.[22,25,26]

(24) Qi, F.; Yang, R.; Yang, B.; Huang, C. Q.; Wei, L. X.; Wang, J.; Sheng, L. S.; Zhang, Y. W. *Rev. Sci. Instrum.* **2006**, *77*, 084101.

(25) Premkumar, P. A.; Bahlawane, N.; Kohse-Hoinghaus, K. *Chem. Vap. Deposition* **2007**, *13*, 219–226.

(26) Premkumar, P. A.; Bahlawane, N.; Reiss, G.; Kohse-Hoinghaus, K. *Chem. Vap. Deposition* **2007**, *13*, 227–231.

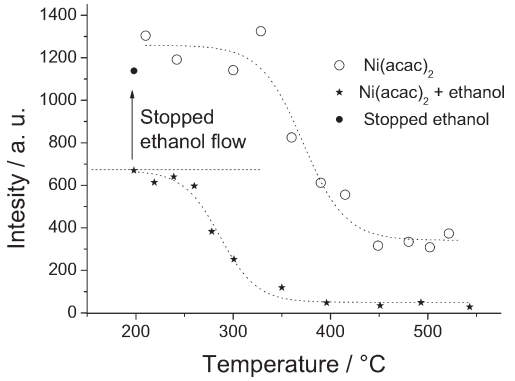

Figure 3. Effect of the addition of ethanol vapor on the thermolysis profile of $Ni(acac)_2$. The ionization energy was set at 11.5 eV and the most intense molecular peak ($m/z = 256$) was monitored.

There, we have shown that high quality thin metallic films can be grown at temperatures that are significantly lower than those needed for the hydrogen reduction route. Thermally stable fcc-nickel films were grown below 300 °C. For example at a substrate temperature of 250 °C, nickel grows with a rate of 6 nm/min, and films with a thickness of 8 nm on glass substrates are already electrically conductive (513 $\mu\Omega$ cm).[27] At low deposition temperature (<200 °C), the metastable hcp-nickel structure is formed with a near-bulk resistivity at thicknesses exceeding 200 nm.[22] In contrast to the conventionally used hydrogen reduction route, ethanol-induced reduction enables growth kinetics without incubation time which leads to a coalescence in early stage of deposition and the formation of electrically conductive ultrathin films; and lower deposition temperature which favors the growth of metastable phases.

Mechanism and Particularities of the Growth Process. Controlling the growth of alloy thin films with the PSE−CVD process requires an accurate understanding of the overall reaction mechanism which is taking place during deposition. Therefore, in situ mass spectrometric analysis was performed to unravel the role of ethanol in the deposition process of nickel thin films. A comparative study of the evaporated $Ni(acac)_2$ precursor from a conventional bubbler and of the precursor delivered with ethanol using the PSE unit shows that no reaction takes place between ethanol and the precursor neither in the liquid feedstock nor during evaporation. Therefore the deposition process is not likely to involve gas-phase reactions. Increasing the substrate temperature, while in situ analyzing the gas sampled after its interaction with the hot substrate surface shows that the thermolysis of $Ni(acac)_2$ significantly takes place at 350 °C, however the total decomposition was not attained even at temperatures exceeding 500 °C. The thermolysis leads to the formation of acetylacetone, propene, and other hydrocarbons as illustratively shown in the Supporting Information (SI). Introducing a coflow of ethanol clearly decreases the thermolysis temperature and a complete depletion of $Ni(acac)_2$ was already observed at 400 °C as depicted in Figure 3. The introduction of ethanol vapor leads also to a significant decrease of the precursor intensity which is attributed to the dilution effect. In fact, the flow of added ethanol was calculated to be 1.5 slm, which is expected to cause a loss of 64% of the intensity of the precursor signal.

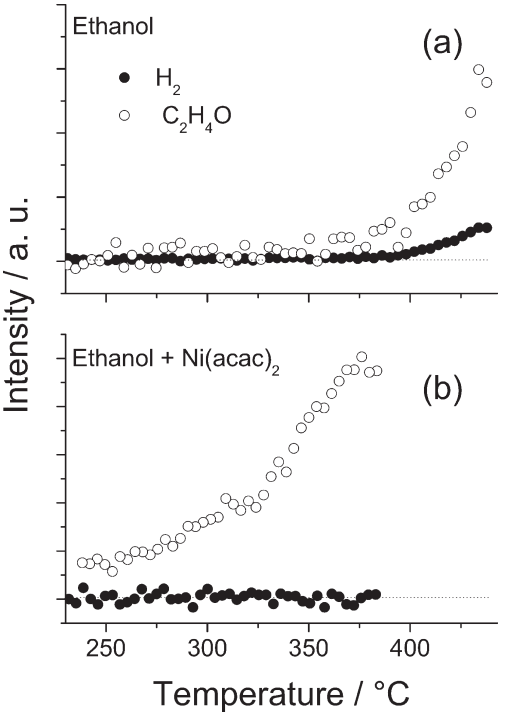

Figure 4. Mass spectrometric monitoring of the molecular peaks of the products of the oxidative dehydrogenation of ethanol as a function of the temperature in the absence and in the presence of nickel acetylacetonate. The ionization energy was set at 16.5 eV to enable the detection of hydrogen.

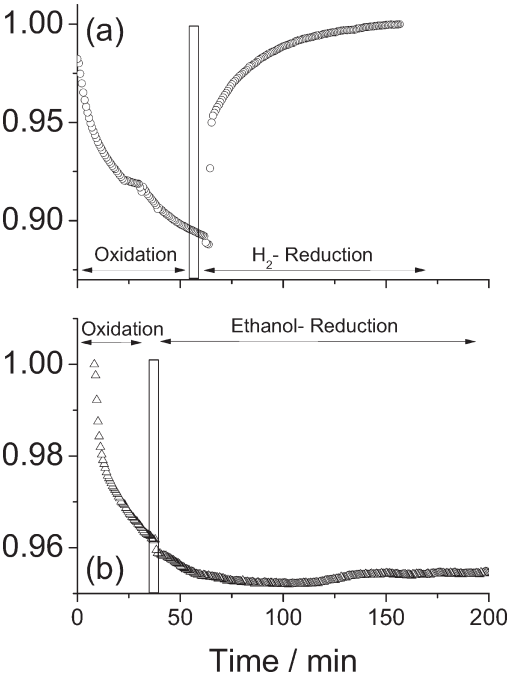

Figure 5. Infrared monitoring of the oxidation, at 280 °C, of a 14 nm thick nickel films grown on glass, and the subsequent reduction of the oxidized surface by hydrogen (a) or ethanol (b) vapor in vacuum (30 mbar).

(27) Premkumar, P. A.; Turchanin, A.; Bahlawane, N. *Chem. Mater.* **2007**, *19*, 6206–6211.

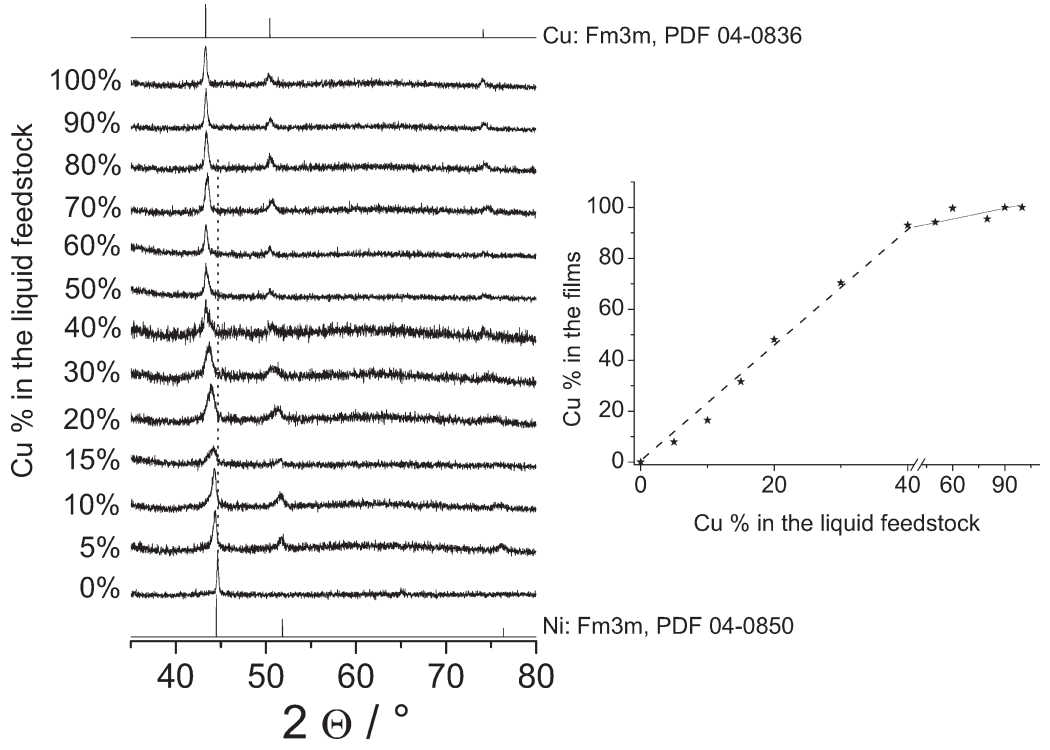

Figure 6. XRD profiles of Ni−Cu alloy thin films grown on glass substrates, and the dependence of their composition on that of the liquid feedstock used for deposition by CVD.

The investigation of the effect of $Ni(acac)_2$ on the thermolysis of ethanol was studied with mass spectrometry and the obtained results are depicted in Figure 4. In a clean reactor, ethanol also decomposes above 380 °C to form acetaldehyde and molecular hydrogen. In the presence of $Ni(acac)_2$, acetaldehyde was significantly formed already at a temperature of 240 °C, however, no molecular hydrogen was detected even at temperatures exceeding 350 °C indicating its transfer to the acetylacetonate ligand of the nickel precursor. The formation of acetylacetone, results shown in the SI, was observed at low temperature, whereas methane was significantly observed above 350 °C indicating the further decomposition of the ligand moiety, which is associated with high risk of carbon contamination.

The mass spectrometric investigation shows that the reduction of nickel acetylacetonate occurs at the deposition surface without prior gas-phase reactions. The adsorbed nickel precursor activates the dehydrogenation of ethanol, and the abstracted hydrogen atoms are transferred to the acetylacetonate ligand. As a result, the steady deposition proceeds via the ligand release from the adsorbed precursor as acetylacetone, and the requested hydrogen atoms are gained from the conversion of ethanol to acetaldehyde. In an advanced stage of deposition, the formed nickel layer is eventually expected to induce the catalytic decomposition of ethanol. However, such a reaction was reported only at temperatures above 400 °C,[28] leading to the formation of fibrous carbon deposit. Therefore, a well controlled growth of nickel from the ethanol-induced reduction of $Ni(acac)_2$ is favorably obtained at the temperature window of 185−400 °C.

The low-temperature reactivity of ethanol with metal acetylacetonates enables the growth of metallic layers even on highly reducible metal oxides such as nickel oxide, a property that is expected to widen the application of metallic thin and ultrathin films. To simulate a nickel oxide surface, the metallic nickel layer was first grown on glass substrate and then oxidized in a controlled way under IR in situ monitoring. In a first step the exposure of the nickel layer to air atmosphere at 280 °C leads to a slow oxidation kinetics, and the reflection of IR radiation (2500 cm^{-1}) shows a continuous decay as illustrated in Figure 5a and b. In a second step, the oxidized surface was exposed to hydrogen or to ethanol vapor to investigate their reactivity. Figure 5 demonstrates that ethanol, in contrast to molecular hydrogen, does not reduce nickel oxide under realistic deposition conditions which preserves the properties of the underlying substrate for specific applications such as eletrocatalysis. Therefore, this study shows that, relative to molecular hydrogen, ethanol exhibits a superior affinity toward the reduction of nickel acetylacetonate in CVD conditions, whereas it remains nonreactive toward oxide surfaces, enabling efficient and mild deposition conditions for metallic nickel.

Nickel−Copper Alloys. The deposition of Ni−Cu alloys was performed under conditions where both nickel and copper thin films grow in the cubic structure with the Fm3m symmetry as shown in Figure 6. Pure copper and nickel films are polycrystalline, however, nickel thin films

(28) Red'kin, A. N.; Kipin, V. A.; Malyarevich, L. V. *Inorg. Mater.* **2006**, *42*, 242–245.

show a marked (111), $2\theta = 44.5$, orientation that is lost when a small amount of copper is introduced into the lattice. Upon the increase of the fraction of copper in the liquid feedstock, the XRD diffraction peaks show a steady shift to low diffraction angles, indicating the insertion of copper into the lattice of nickel. This shift proceeds until the characteristic diffraction pattern of copper is obtained which indicates the unlimited solubility of copper in nickel.

The analysis of the films composition, insert of Figure 6, shows that the fraction of copper in the deposited film increased linearly with its fraction in the liquid feedstock, which enables the attainment of Ni−Cu alloy thin films with virtually any composition. Nevertheless, all films obtained with liquid feedstocks of a copper fraction exceeding 0.4 contain more than 94% of copper. In this range, copper content in the films increases very slightly with that in the liquid feedstock. This behavior was unexpected since the growth rate of nickel is 3-fold that of copper.[25] The deposition rate of copper-rich films from feedstocks containing more than 40% of copper acetylacetonate is significantly higher than that obtained with feedstock containing only copper. Since the overall metal concentration in the feedstock is maintained constant, this observation can be attributed to an eventual nickel-catalyzed deposition of copper.

The morphology of pure nickel consists of densely packed large crystallites. The formed alloys exhibit morphologies that are very sensitive to the amount of incorporated copper, as illustrated in Figure 7. Nickel-rich films are formed by less-densely packed crystals that are significantly smaller than those observed for pure nickel. This observation corroborates with the significantly broadened XRD diffraction peaks in Figure 6. Films of copper-rich compositions present coarse morphology with heterogeneously distributed particle size compared to nickel-rich alloys. Interestingly near a Ni/Cu ratio of 1, films exhibit a structure with the highest apparent density. SE-micrographs with lower magnifications are available as SI.

Nickel−Cobalt Alloys. Referring to our previous work[27] with the CVD-based alcohol reduction process, metallic cobalt thin films were only grown in the hcp structure. The choice of the alcohol and of the deposition temperature enables the growth of either metallic cobalt or carbide (Co_2C).[27] Metallic cobalt thin films were obtained using propanol as reducing agent and a deposition temperature of 250 °C or above, whereas Co_2C grew using ethanol feedstock and deposition temperatures below 230 °C.

In contrast to cobalt, the growth using alcohol feedstocks of nickel acetylacetonate leads only to metallic nickel deposits. The metastable hexagonal structure (hcp) was obtained at deposition temperatures below 200 °C,[22,23,26] while the stable cubic structure (fcc) grew at higher temperatures.[22,23] Based on these preliminary results, it is clear that there are no common conditions for the growth of metallic nickel and cobalt in the same crystalline structure. Therefore, the growth of Ni−Co alloy is expected to be possible in a limited composition range.

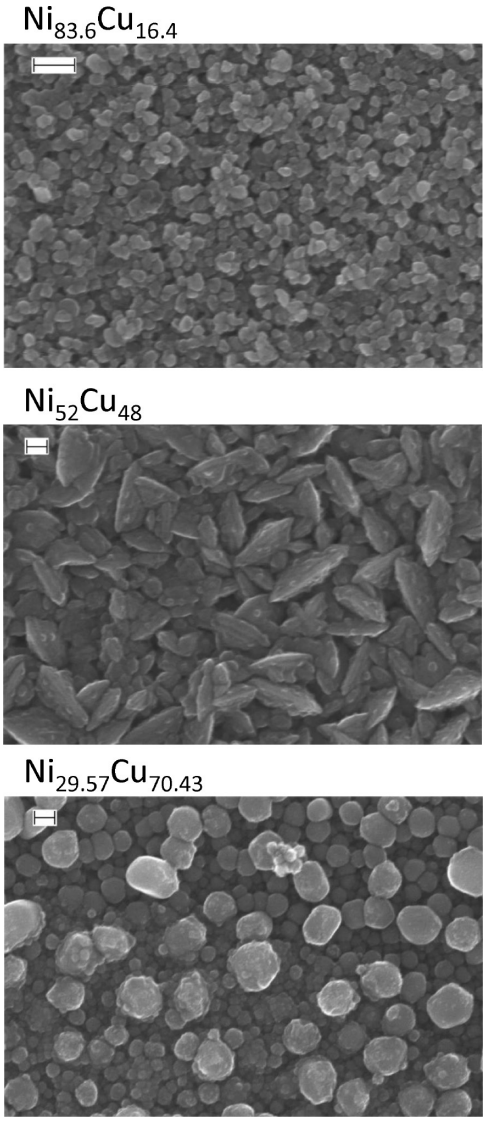

Figure 7. SE-Micrographs of selected Ni−Cu alloy compositions. The scale bar corresponds to 200 nm in the first micrograph ($Ni_{83.6}Cu_{16.4}$) and to 100 nm in the other cases.

The XRD profile, Figure 8, of the grown nickel thin films at 190 °C, starting from ethanol solution of nickel acetylacetonate, shows the hcp structure with relative intensities that compare well to the polycrystalline diffraction database. Introducing cobalt acetylacetonate into the ethanol feedstock causes a regular shift of the diffraction peaks, as depicted in the insert (a) of Figure 8, as a function of the composition of the resulting film. The insert (b) shows a linear dependence between the composition of the liquid feedstock and that of the resulting films which can be conveniently exploited to provide a high control of the Ni−Co film composition. A substantial deviation from this linearity is only observed for cobalt-rich feedstocks, resulting in a preferential incorporation of cobalt as a carbide crystalline phase. In fact, the regular shift of the diffraction peaks with cobalt fraction in the film is already significantly affected for Co/(Co+Ni) = 0.275, showing the upper limit of

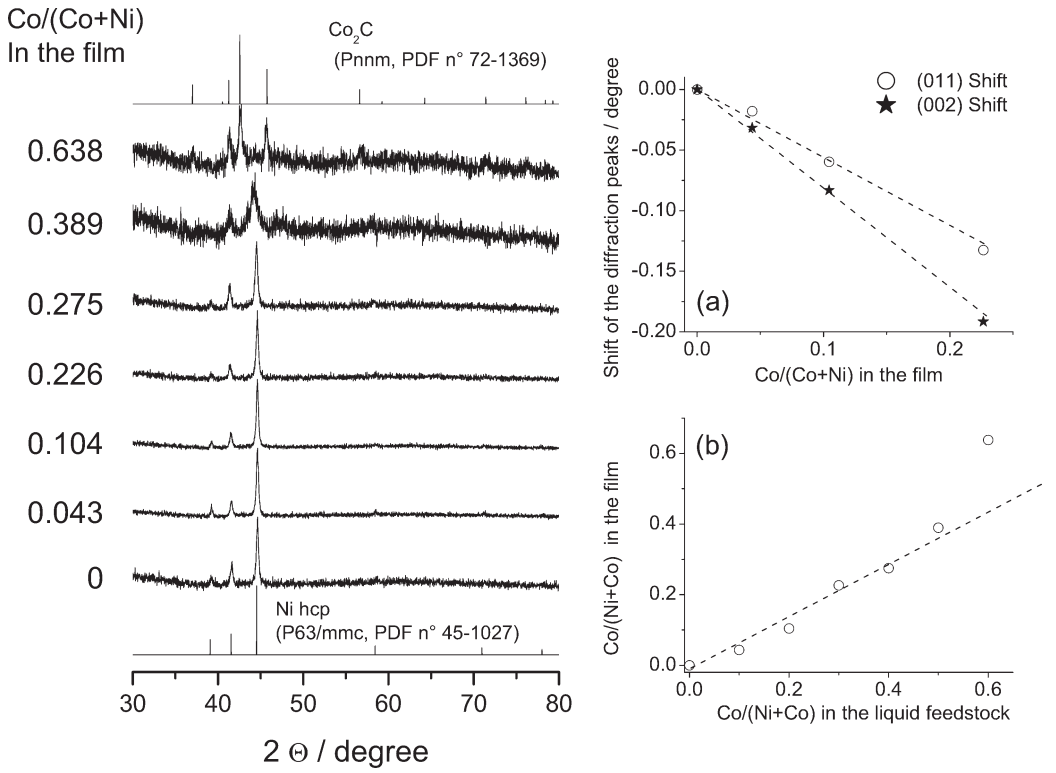

Figure 8. XRD profiles of Ni−Co alloy thin films grown on glass substrates. The insert (a) shows the shift of the diffraction peaks (002) $2\theta = 41.5°$ and (011) $2\theta = 44.5°$ with the composition of the obtained films. The dependence of the composition of the film on the composition of the liquid feedstock is depicted in the insert (b).

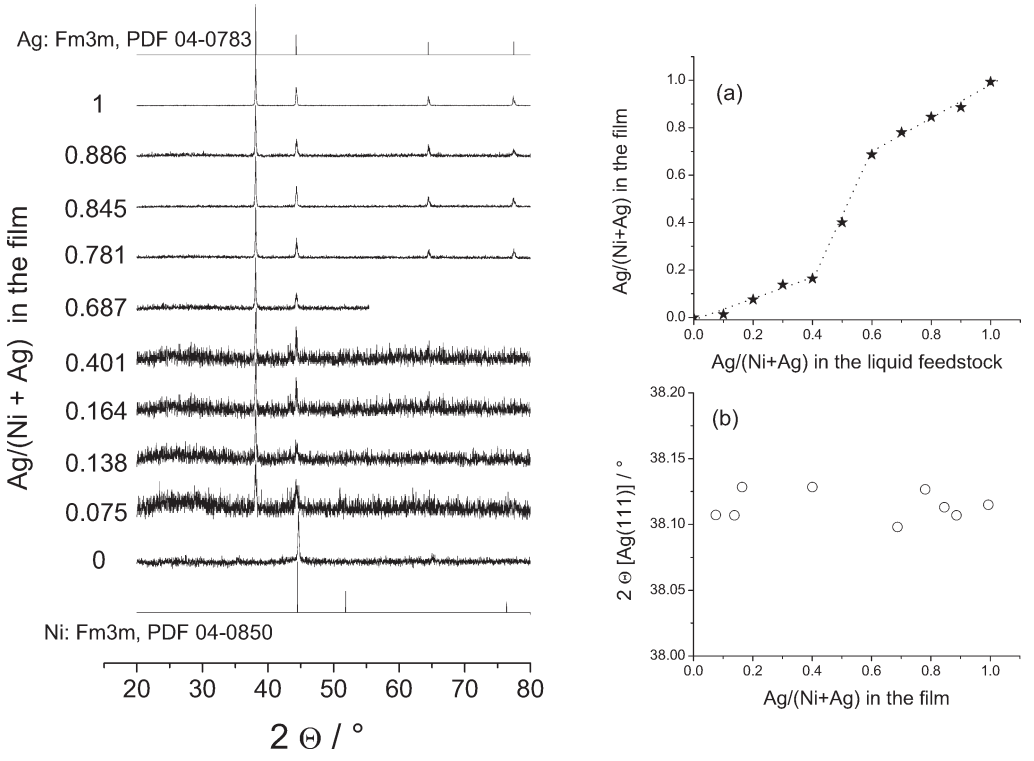

Figure 9. XRD profiles of Ni−Ag thin films grown on glass substrates. The insert (a) shows the variation of the film composition as a function of that of the liquid feedstock and the insert (b) shows the diffraction angle of Ag(111) as a function of the film composition.

Ni−Co synthesis in the hcp structure under the presently investigated deposition conditions. Higher content of cobalt in the feedstock leads to a deposit with poor crystallinity and then to the formation of a carbide phase.

Nickel−Silver Alloys. The growth of Ni−Ag thin films was performed at a substrate temperature of 350 °C and a pressure of 50 mbar. The ratio of $AgNO_3$ to $Ni(acac)_2$ was adjusted in the liquid feedstock while the total metal

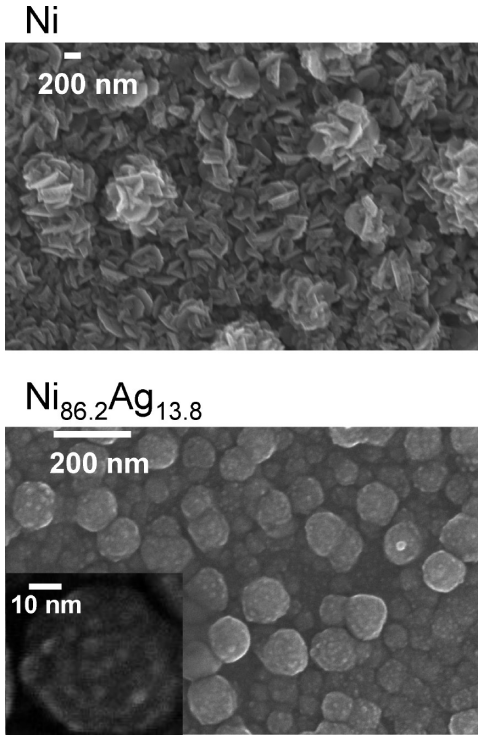

Figure 10. SE-Micrographs of the deposited pure nickel and nickel films containing a silver fraction of 0.138.

concentration was kept at 5×10^{-3} mol/L. The insert (a) in Figure 9 shows the variation of the film composition as a function of the composition of the feedstock. These results show clearly that the composition of the film can be well controlled by adjusting the composition of the liquid feedstock; nevertheless, two ranges can be distinguished. The observed trend shows that feedstocks with nickel fractions higher than 0.6 lead to an incorporation of silver in the film that is moderate relative to its concentration in the feedstock. In fact the ratio χ_{Ag}(film)/χ_{Ag}(feedstock) in this range is equal to 0.45, where χ_{Ag} is the atomic fraction of silver. Similar observation was noticed for feedstocks with silver fractions higher than 0.6, where χ_{Ni}(film)/χ_{Ni}(feedstock) ratio was calculated to be 0.72. The XRD patterns of the obtained films show that all films, except pure nickel, exhibit the diffraction pattern of silver. Furthermore, the insert (b) of Figure 9, shows that the diffraction peaks of the crystalline silver phase do not exhibit any shift with the variation of the film composition, which indicates that nickel does not dissolve in the lattice of silver. Therefore, nickel is supposed to form either an amorphous or nanocrystalline phase. The XRD data show that introducing a silver fraction as low as 0.075 hinders completely the formation of detectable nickel crystallites, while pure crystalline silver was detected. Therefore it is assumed that a silver fraction far below 0.075 is able to incorporate into the lattice of nickel and limit the growth of detectable crystallites by XRD.

The SEM inspection of the surface of the deposited nickel film shows that nickel forms a compact morphology made of platelets-like crystallites with size exceeding 200 nm as shown in Figure 10. Nickel film containing a silver fraction of 0.138 shows a dramatic modification of the film morphology. The obtained film in this case exhibits large spherical particles, presumably Ag, that are decorated by nanoparticles possessing an average size of 7 nm. These nanoparticles are expected to be the nickel phase that is not detected by XRD. Even though no experimental evidence can be given at this stage, the fact that small fraction of silver is able to hinder the growth of nickel crystals might be reasonably attributed to the incorporation of some silver into the lattice of nickel which generates a large stress and limits their further growth. Assuming the core−shell structure, where nickel-rich nanoparticles constitute the shell, it is very likely that the EDX analysis shown in Figure 9a overestimates the content of nickel.

Conclusions

The present work provides insight into the role of ethanol in the deposition of metallic nickel in hydrogen-free atmosphere using the thermally activated PSE−CVD process. The key reaction, which is the dehydrogenation of ethanol and the transfer of atomic hydrogen to the ligand, takes place at temperatures where both the precursor and ethanol are thermally stable. Ethanol was shown to be nonreactive toward nickel oxide which means on one side that the reaction to metallic nickel is unlikely to proceed if the precursor is already decomposed to form a nickel oxide-like deposit. On the other side, this result shows that the deposition process involving ethanol provides mild deposition conditions so that even highly reducible oxides like NiO can be used as substrates, which contrasts with the H_2-reduction route.

Thin films of Ni−Cu alloy were grown with controlled compositions taking benefit from the advantages of the liquid delivery. The solubility between nickel and copper allowed the attainment of fcc−$Ni_{1-x}Cu_x$ with $0 \leq x \leq 1$. Regarding Ni−Co alloys, the possibility to grow nickel thin films with the hcp structure has enabled the deposition of metastable nickel-rich Ni−Co compositions in the hcp structure. These phases might present magnetic and magneto-electric properties that contrast with those of the fcc counterpart. Introducing high amount of cobalt in these conditions was shown to favor the formation of a single carbide phase.

In the case of Ni−Ag alloys, it was shown that incorporating small amount of silver during the deposition of nickel completely hinders the growth of nickel crystallites and particles with sizes of 7 nm were formed. Therefore alloying with a small amount of silver might be regarded as an efficient way to obtain films composed of nickel particles with sizes below 10 nm. The XRD analysis shows only the formation of the pure silver crystalline phase.

The present study shows that the CVD process offers mild deposition conditions for the highly controlled growth of a large variety of alloys with a great flexibility in terms of composition. Furthermore, the growth of metastable structures such as the hcp nickel-rich

Ni−Co alloy thin film opens the possibility toward the investigation of structure-dependent properties of alloys.

Acknowledgment. We are grateful for the financial support of the German Academic Exchange Service (DAAD: PKZ: D/0600357) and the Ministry of Science and Technology of China (2007DFA61310). P.A.P. acknowledges a fellowship of the Alexander von Humboldt (AvH) foundation.

Supporting Information Available: The decomposition of the precursor at high temperature to form methane. The contrast between the thermolysis and the reaction with ethanol in terms of production of propene as product. SEM micrographs of Ni−Cu alloys representing various magnifications. This material is available free of charge via the Internet at http://pubs.acs.org.